Capillary Condensation in Porous Materials. Hysteresis and Interaction without Pore Blocking/Percolation Process

Annie Grosman, Camille Ortega

Capillary Condensation in Porous Materials. Hysteresis and Interaction Mechanism without Pore Blocking/Percolation Process

Annie Grosman* and Camille Ortega

Institut des Nanosciences de Paris (INSP), Universités Paris 6, UMR-CNRS 75-88, Campus Boucicaut, 140 rue de Lourmel, 75015 Paris, France

Received December 19, 2007. In Final Form: January 29, 2008

We have performed measurements of boundary hysteresis loops, reversal curves, and subloops in p^+-type porous silicon, a porous material composed of straight non-interconnected pores. These data show that a strong interaction mechanism exists between the pores. The pores of porous silicon are non-independent, whereas they are not interconnected. This hysteretic behavior is very similar to that observed in porous glass, which consists of cavities connected to each other by constrictions. This questions the so-called pore blocking/percolation model developed to explain the behavior of fluid in porous glass. More generally, if we disregard the shape of the boundary hysteresis loops which depends on the porous material (H1 for MCM-41 and SBA-15, H2 for porous glass and p^+-type porous silicon), the hysteretic features inside the main loop are qualitatively the same for all these porous systems. This shows that none of these systems are composed of independent pores. A coupling between the pores is always present whether they are interconnected or not and whatever the shape of the main loop is.

1. Introduction

In a previous letter,[1] we have reported on the presence of hysteresis loop of type H2 (IUPAC classification[2]) in the adsorption−desorption isotherms of gas in p^+-type porous silicon. This type of hysteresis loop, asymmetrical with an evaporation branch steeper than the condensation branch, is generally considered as the signature of the occurrence of a percolation process during the emptying of disordered porous material[2−6] such as porous glass or silica aerogel, which consist of cavities connected to one another by constrictions, most of the cavities having no direct access to the gas reservoir. This is conventionally explained by the pore blocking/percolation model developed by Mason[5,6] to reproduce the family of adsorption−desorption isotherms obtained by Brown in porous glass.[7] The observation of such a hysteresis in p^+-type porous silicon was unexpected because this porous material is composed of non-interconnected tubular pores all being in direct contact with the gas reservoir, a morphology very different from that of porous glass or silica aerogel. We have thus questionned the pore blocking/percolation process to be the cause of the observed hysteresis.

In the present paper we come back to these experiments with more details than in the letter. In particular, we measure reversal curves and subloops inside the main loop to confirm what was suggested by the asymmetry of the boundary hysteresis loop: in porous silicon the pores do not empty independently of one another but through a cooperative process. These experimental data are analyzed carefully under the pore blocking/percolation model. Let us briefly outline this model.

Consider first an isolated pore separated from the gas reservoir by a constriction (or neck), the so-called ink-bottle pore (Figure 1). According to the pore blocking model, the pore body can empty only when the constriction empties. Thus, the evaporation pressure of the pore body does not depend on its size but only on the size of the constriction and is delayed with regard to its condensation pressure, giving rise to a hysteresis phenomenon (Figure 1a).

In an assembly of non-interconnected ink-bottle pores we should observe a hysteresis loop with condensation and evaporation branches characteristic of the distributions of the pore size and of the neck size, respectively. The global hysteresis loop should be the sum of the individual hysteresis loops. In such a system there is a priori no reason to observe a hysteresis loop of type H2. For example, the hysteresis loop schematically represented in Figure 1b corresponds to a neck size distribution as large as that of the pore body in relative terms, the pressure p^* being the evaporation pressure of the largest neck. If the evaporation is commenced when the porous system is not fully filled, none of pores can empty before this pressure is reached and the curves expected, called primary desorption scanning curves (PDSCs), are schematically represented in Figure 1b.

Consider now an assembly of cavities connected together by constrictions which is the case of disordered porous materials such as porous glass or silica aerogel. Such a morphology is schematically represented in inset of Figure 2. Most of the cavities are located within the porous material and have no direct access to the gas reservoir but indirect access through many constrictions and cavities. Thus, if evaporation is commenced when the porous system is completely filled, a cavity cannot empty as long as a continuous vapor path is not created to the cavity from the vapor reservoir. But, as soon as the pressure is reduced to some critical value (p^* in Figure 2), the porous system begins to empty and many routes are created from the vapor reservoir to the buried pores which result in the emptying of the whole system in a cascade-like manner. Thus, the emptying of a disordered porous material is believed to take place through a percolation process explaining the asymmetrical shape of hysteresis loop (Figure 2). If now the evaporation process is commenced when the porous

* To whom correspondence should be addressed. E-mail: annie.grosman@insp.jussieu.fr.

(1) Coasne, B.; Grosman, A.; Ortega, C.; Simon, M. *Phys. Rev. Lett.* **2002**, *88*, 256102.
(2) Gregg, S. J.; Sing, K. S. W. *Adsorption, Surface Area and Porosity*; Academic Press: London, 1982; Chapter 3, p 111.
(3) Everett D. H. *The Solid Gas Interface*; Dekker, Flood: New York, 1967; Vol. 2, Chapter 36, p 1055.
(4) Rouquerol, F.; Rouquerol, J.; Sing, K. *Adsorption by powders & porous solids*; Academic Press: San Diego, 1999.
(5) Mason, J. *Proc. R. Soc. Lond.* **1983**, *A390*, 47.
(6) Mason, J. *Proc. R. Soc. Lond.* **1988**, *A415*, 453.
(7) Brown, A. J. *Thesis, Bristol* **1963**.

10.1021/la703978v CCC: $40.75
Published on Web 03/15/2008 PAGE EST: 9.1

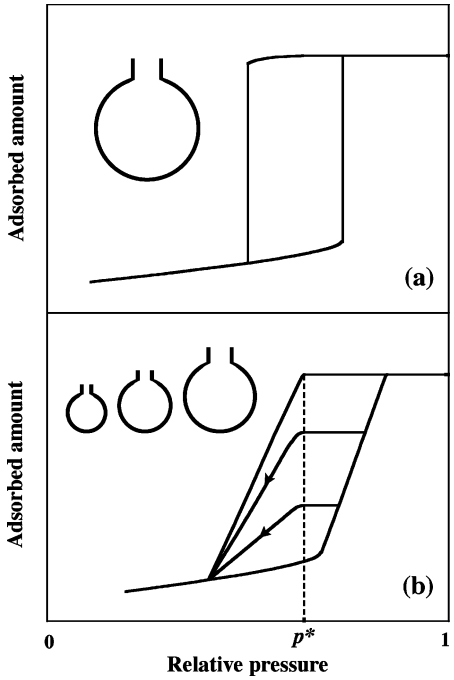

Figure 1. (a) Hysteresis loop for an ink-bottle pore. (b) Hysteresis loop for an assembly of non-interconnected ink-bottle pores with random size distributions of cavities and necks; two primary descending scanning curves (PDSCs) are represented. Along these PDSCs, none of pores can empty above p^*, the evaporation pressure of the largest necks.

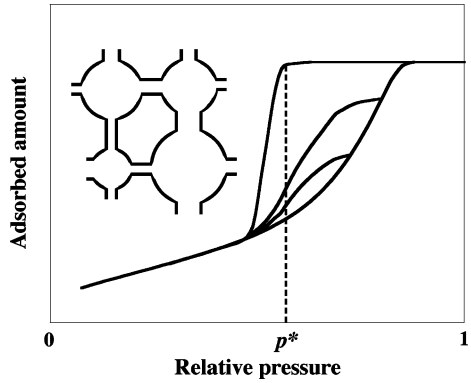

Figure 2. Schematic hysteresis loop of type H2 and PDSCs for porous glass, an assembly of cavities connected by constrictions as represented in the inset. According to the pore blocking/percolation model, evaporation along the PDSCs can occur at pressure higher than p^*, the evaporation pressure of the system when it is fully filled which is the signature of the occurrence of a percolation process.

system is not completely filled, a filled cavity can have a neighboring empty cavity, so that it can empty into this empty cavity, the desorbed material being carried by a series of condensation−evaporation steps to the bulk vapor.[5] Therefore, the hysteretic behavior of a filled cavity depends on whether the adjacent cavities are filled or empty and the shape of the obtained PDSCs are different from that of the boundary evaporation branch. In Figure 2, we have represented typical PDSCs observed in porous glass. Thus, it is believed that the observation of the hysteresis loop of type H2 and of the PDSCs represented in Figure 2 is the signature of the occurrence of a percolation process in disordered porous materials.

The present paper is organized as follows. Section 2 presents the techniques for making the porous silicon samples and measuring their properties such as porosity, morphology, pore size, etc. Adsorption measurements are also presented. In Section

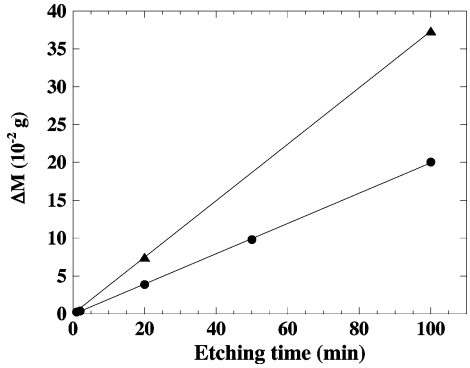

Figure 3. $\Delta m_{12} = m_1 - m_2$ (●), the mass of the removed silicon atoms, and $\Delta m_{13} = m_1 - m_3$ (▲) which is proportionnal to the thickness of the porous silicon layer, versus the etching time. The electrochemical conditions are those of sample A (see Table 1). The etching rate is ∼1 μm/min. The surface area of the Si wafer electrochemically etched equals 15.2 cm^2.

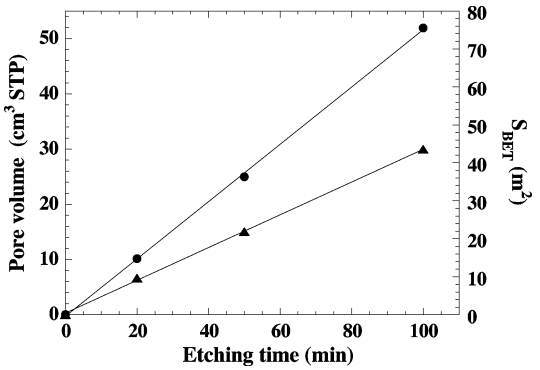

Figure 4. Pore volume measured on the saturation plateau of N_2 adsorption isotherms performed at 77.4 K (●) and BET surface area (▲) for porous silicon layers prepared under the same electrochemical conditions as sample A (see Table 1) versus the etching time. The etching rate is ∼1 μm/min, and S_{BET} is 266 m^2/g. The surface area of the Si wafer electrochemically etched equals 15.2 cm^2.

3.1, we discuss whether the irreversibility of the capillary condensation is due to the presence of constrictions in the porous material (pore blocking). In Section 3.2, we present and discuss measurements of PDSCs and subloops between the same pressure end points within the main loop which is another test of the independence of the pores. These results unambiguously prove that there exists a strong interaction mechanism between the pores during the evaporation. The relevance of percolation process in this system is discussed and ruled out.

2. Experimental Section

Mesoporous silicon layers are prepared by anodic dissolution of highly boron doped (100) Si single crystal in hydrofluoric acid/ethanol solutions (HF/EtOH). Thus, one obtains samples with a porous part supported by a silicon substrate, i.e., with pores closed at one end.[8] Two macroscopic parameters, the porosity and thickness of the porous layers, are measured by weighing with a microbalance (precision of ±0.5 μg) the samples before (mass m_1) and after (m_2) the electrochemical etching and after removal of the porous part in NaOH solutions (m_3). The porosity is given by the ratio $(m_1 - m_2)/(m_1 - m_3)$ and the thickness is proportional to $(m_1 - m_3)/\rho$ where ρ is the silicon density. The porosity depends on the HF concentration and the current density (J), while the thickness is controlled by the etching time.

(8) Grosman, A.; Ortega, C. In *Structural and Optical properties of Porous Silicon Nanostructures*; Amato, G., Delerue, C., Von Bardeleben, H. J., Eds.; Gordon and Breach Science Publishers: London, 1997; Vol. 5 Chapter 11, p 317.

Table 1. Structural Parameters of Porous Silicon Layers as a Function of the Formation Conditions[a]

porous layer	J (mA/cm^2)	HF/EtOH	etching time (min)	porosity	thickness (μm)	pore density (10^{11} cm^{-2})	S_{TEM} (m^2/g)	S_{BET} (m^2/g)
sample A	20	3:1	20	51.4%	21.2	3.7	138	266
sample B	50	1:1	10	70.8%	18.4	1.2	164	285

[a] the surface area of the Si wafer electrochemically etched is 15.2 cm^2. the porous layers are prepared from p$^+$-type (3.10^{-3} Ω·cm) [100] Si substrates. the BET surface areas are given in (1/g adsorbent), i.e., (1/g porous layer).

We have prepared several porous layers under the same electrochemical conditions, i.e., for a given couple of values (HF concentration, J), but with different etching times. Figure 3 shows that $\Delta m_{12} = m_1 - m_2$, the mass of the removed silicon atoms, and $\Delta m_{13} = m_1 - m_3$, which is proportional to the porous layer thickness, vary linearly with the etching time. These results indicate that the chemical and lateral electrochemical etchings of the silicon wall surface are negligible compared to the frontal etching and hence prove the absence of a porosity gradient.

We get complementary information about the formation process by studying the nitrogen adsorption isotherms. Figure 4 shows that the pore volume, measured on the saturation plateau of the isotherms, and the surface S_{BET}, deduced from the BET model analysis,[9] are proportional to the etching time. Values of the pore volume are systematically a few percent (4−5%) lower than values deduced from the weight measurements according to $\Delta m_{12}/\rho$. This is due to the presence of a monolayer of SiHx (x = 1, 2, or 3) groups on the Si pore walls,[10−12] undetectable by weighing. These results show that the whole pore volume is accessible for ambient molecules.

For this study, two types of porous layers were prepared, ~20 μm thick, with porosity face values of 50% (sample A) and 70% (sample B). Table 1 summarizes the formation condition parameters together with the porosity, thickness, pore density, and S_{BET} values of these layers.

Previous transmission electron microscopy (TEM) studies of sample A have shown that these media exhibit an ordered porous morphology with tubular pores parallel to one another and perpendicular to the (100) plan of the Si substrate.[1,8] It has been shown[13] by proton energy loss fluctuation measurements that the average direction of the pores is identical to within ±0.1° of the [100] crystal axis. The pores of polygonal cross sections are separated by Si single-crystal walls of apparent constant thickness (see the TEM plane view in ref 1 for sample A and Figure 5a for sample B). We have also shown[1] the absence of lateral interconnection between the pores.

From a numerical treatment of TEM plane views, it is possible to estimate the pore size distribution (PSD) of the layer. We make a binary image of the corresponding negative TEM photograph by adjusting the threshold value to reproduce, as faithfully as possible, the number and shape of the pores. The porous layers are thinned down to 100−200 nm by mechanical polishing and ion milling. The TEM plane view is performed on the bevelled part of the side of the crater produced by the ion milling process. It is hence only natural that the obtained binary image does not reproduce exactly the porosity and the consistancy in the silicon wall thickness. Therefore, we decide to skeletonize the binary image and then to apply a spatial convolution using a kernel matrix (Laplacian matrix 3 × 3) to thicken uniformly the silicon walls until the porosity of the sample is reproduced. Figure 5b shows the obtained result. It is noteworthy that the two images of Figure 5a and b are quite superimposable. The PSD corresponding to cylindrical pores having the same cross-section area as the polygonal pores is shown in Figure 5c together with that obtained by a similar treatment of a TEM image of sample A. The PSDs, with large standard deviations, are both centered on the mean value of the pore size, ~13 ± 6 and ~26 ± 14 nm for samples A and B, respectively. The PSD measurements were found to be reproducible to within 10% about. Note that the PSDs corresponding to cylindrical pores having the same perimeter value as the polygonal pores are quite similar to those shown in Figure 5c, indicating that the pore section is rather regular than oblong.

The fact that the 2D image (see Figure 5a) perpendicular to the pore axis yields the same porosity as that obtained by weighing which corresponds to the 3D morphology is a strong argument against the presence of numerous constrictions and indicates that the cross section area of each pore is almost constant. However, previous electronic paramagnetic resonance studies of p$^+$-type porous layers[14] have shown the presence of dangling-bonds located on (100), (110), and (111) Si surfaces at the Si/SiO$_2$ interfaces. This result displays the presence of {100}, {110}, and {111} facets on the Si walls, i.e., a roughness at the atomic scale. The presence of these facets is not surprising if we consider the polygonal shape of the pores formed in a (100) Si substrate. In Table 1, we give the surface areas calculated from the total pore perimeter l, $S_{TEM} = lL$ where L is the pore length. S_{TEM} is about two times lower than S_{BET}. S_{TEM} evidently underestimates the true surface area since it neglects the presence of roughness at the scale of a few atoms that we mentionned above. S_{BET} probably overestimates the true surface area because the adsorbate accumulates in the corner of the pores to decrease the interface adsorbate/vapor area.

The consistancy in the Si wall thickness and the absence of a porosity gradient indicate that these walls exhibit a high electrical resistivity, compared to that of the substrate, which avoid them to be further etched. We have shown[11,12] that this high resistivity[15] is neither due to the absence of dopant (boron) atoms nor to their passivation by hydrogen atoms. The causes of such a high resistivity are not yet very well understood. What we know is that the Si/HF interface plays a fundamental role in this property since the Si walls remain electrically resistive as long as the HF solution is present. To render the Si walls electrically conducting, it is necessary to exchange the HF/EtOH solution for a neutral salt (KNO_3 for example) solution. In these conditions an anodic oxide film can be formed on the Si wall surface.[16]

This electrical property of the porous silicon layers can be used to make porous silicon membranes with tubular pores open at both ends. Immediately after the porous layer formation, the current density is increased to a value corresponding to the electropolishing regime, without changing the other experimental conditions. During this step, because of the high resistivity of the pore walls, the electric field lines are focused on the bottom of the pores where the Si walls are dissolved. Consequently, the morphology and sizes of the pores in the porous membrane thus obtained are unchanged compared to those of the corresponding porous layer. This is confirmed by studies of adsorption isotherms which will be presented in other papers.[17,18]

Measurements. The adsorption−desorption isotherms, scanning curves, and subloops have been measured using a Micromeritics ASAP2010 instrument equipped with three pressure transducers with full scales of 1 μmHg, 10 mmHg, and 1000 mmHg. We can link

(9) Brunauer, S.; Emmett, P. H.; Teller, E. *J. Am. Chem. Soc* **1938**, *60*, 309.
(10) Grosman, A.; Ortega, C.; J.; M. *J. Appl. Phys.* **1993**, *74*, 1992.
(11) Grosman, A.; Ortega, C. In *Properties of Porous Silicon*; Canham, L., Ed.; INSPEC Publishers: Ipswich, MA, 1997; Chapter 11, p 328.
(12) Grosman, A.; Ortega, C. In *Structural and Optical properties of Porous Silicon Nanostructures*; Amato, G., Delerue, C., Von Bardeleben, H. J., Eds.; Gordon and Breach Science Publishers: London, 1997; Vol. 5 Chapter 13, p 375.
(13) Amsel, G.; d'Artemare, E.; Battistig, G.; Morazzani, V.; Ortega, C. *Nucl. Instr. Methods B* **1997**, *122*, 99.
(14) von Bardeleben, H. J.; Stievenard, D.; Grosman, A.; Ortega, C.; Siejka, J. *Phys. Rev. B* **1993**, *47*, 10899.
(15) Ben Chorin, M. In *Properties of Porous Silicon*; Canham, L., Ed.; INSPEC Publishers: Ipswich, MA, 1997; Chapter 6, p 165.
(16) Grosman, A.; Chamarro, M.; Morazzani, V.; Ortega, C.; Rigo, S.; Siejka, J.; von Bardeleben, H. J. *J.Luminesc.* **1993**, *57*, 13.
(17) Grosman, A.; Ortega, C. To be published.
(18) Grosman, A.; Ortega, C. To be published.

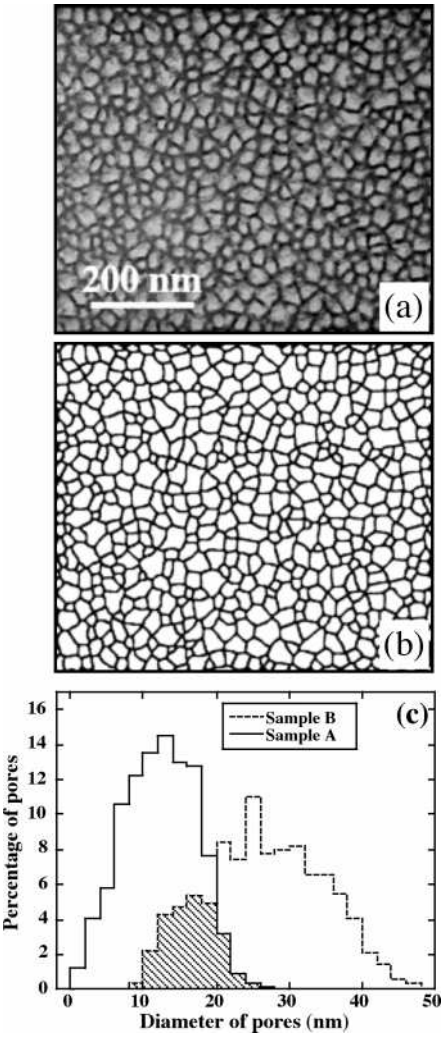

Figure 5. (a) Bright field TEM plane view of a porous Si layer, 70% porosity (sample B), prepared from a p^+-type (100) Si substrate. Observation axis [100]. (b) The corresponding binary image which reproduces both the porosity deduced by weighing and the consistancy in the Si wall thickness. (c) The PSDs, corresponding to cylindrical pores having the same cross section area as the polygonal pores, for samples A and B. The hatched region represents the overlap of the two PSDs.

the classical ASAP2010 apparatus and a homemade cryogenic refrigeration system having a specific analysis cell together. This cooling system is composed of a compressor module (helium gas at 200 bar) connected, via an expander module, to a cryostat which allows to perform adsorption studies at constant temperature (±0.1 K) in the range (16 K-ambient). A cell has been made where porous Si samples formed on 2-in. Si wafers can be analyzed. The gas used were nitrogen, krypton, and argon.

3. Results and Interpretations

3.1. Hysteresis without Pore Blocking. Figure 6 shows the nitrogen adsorption isotherms at 77.4 K corresponding to samples A and B, which are composed of pores closed at one end. These isotherms present wide and asymmetrycal hysteresis loops of type H2 with an adsorption branch characteristic of a broad PSD and a steeper evaporation branch.

As a first remark, we see in Figure 6 that the capillary condensation branches of samples A and B have a common pressure range (0.7−0.8). This supports our PSD analysis (Figure 5c) which shows that the two PSDs overlap: pores of a same size have a same condensation pressure. On the other hand, the two evaporation branches are clearly disconnected from each

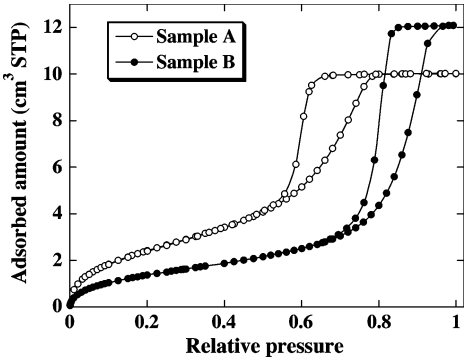

Figure 6. Nitrogen adsorption isotherm at 77.4 K for porous silicon samples A and B, which are composed of pores closed at one end.

other on the whole pressure range, which is a first indication that the evaporation pressures do not depend simply on the individual pore size, that is, the pores in porous silicon are not independent.

The second remark concerns the position of the condensation branches on the pressure axis compared to other porous materials (we disregard the evaporation branch, the status of which is discussed in this paper). For example, the condensation branch for sample A with pores of 13 nm diameter is roughly located at the same pressure as SBA-15 material with cylindrical pores of 8−9 nm diameter,[19] the latter value being deduced from neutron scattering experiments and from mesopore volume determination.[19] The problem has been already pointed out in different papers.[1,20,21] The effect may be partly due to the polygonal shape of the pores but also probably to other phenomena. This question will be treated in a separate paper.

Let us come back to our problem: is the evaporation blocked by the presence of constrictions at the top of the pores?

We have seen in the experimental part that a 2D image perpendicular to the pore axis yields porosity information consistent with that obtained by weighing which corresponds to the 3D morphology. Moreover, the TEM plane view, which is hence representative of the whole porous layer, does not show the presence of constrictions but rather silicon walls of constant thickness. These two results indicate that, if there are constrictions, their spatial extension along the pore axis should be much smaller than the thickness of the membrane analyzed by the electron beam, that is, 100−200 nm in our experiment, and that the volume occupied by the possible constrictions should be much smaller than the pore volume. It is hence conceivable, as stated by Malanoski and co-workers,[20] that constrictions exist in the pores that locally reduce the pore diameter but only for an extremely short distance of the total pore length.

The question is now whether these hypothetical constrictions are concentrated at the top of the pore as it is generally proposed.[20] To answer this question, we have thinned some pieces of sample A, mechanically with an abrasive powder made of silicon carbide balls of 5 μm diameter, or chemically using a $NaOH/H_2O$ solution, to obtain porous layers of different thicknesses: 18.6, 12.9, and 4.3 μm. As the $NaOH/H_2O$ solution cannot enter the pores because dried porous silicon is hydrophobic, the porous layer can be chemically thinned without changing the pore size except at the top of pores as it is shown below. The isotherms have been performed using krypton at 77.4 K which allows to analyze smaller amount of porous material than nitrogen. Figure 7 shows the Kr adsorption isotherms for the three abraded samples and

(19) Grosman, A.; Ortega, C. *Langmuir* **2005**, *21*, 10515.
(20) Malanoski, A. P.; van Swol, F. *Phys. Rev. E* **2002**, *66*, 041603.
(21) Coasne, B.; Grosman, A.; Ortega, C.; Pellenq, R. J. M. *Stud. Surf. Sci. Catal.* **2002**, *144*, 35.

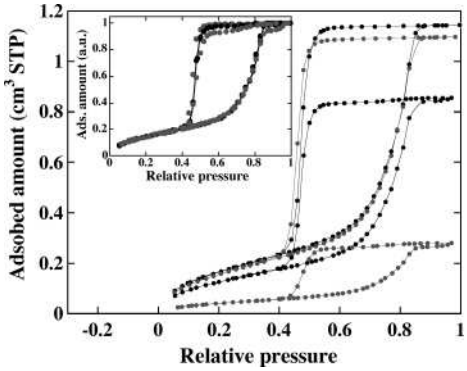

Figure 7. Krypton adsorption isotherms at 77.4 K for sample A as a reference and for the three abraded samples 18.6, 12.9, and 4.3 μm thick, respectively, all normalized to the same geometrical surface as sample A, i.e., to the same number of pores. The inset shows the isotherms normalized to the same pore volume.

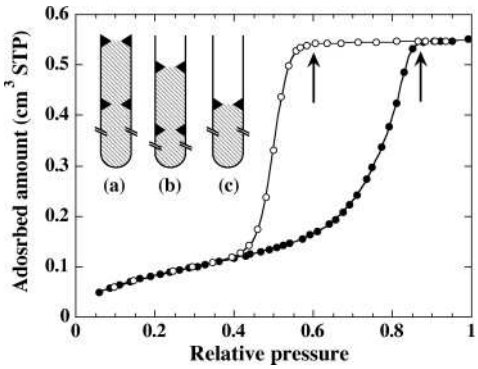

Figure 8. Krypton adsorption isotherm at 77.4 K for a porous layer formed in the same conditions as sample A but 1 μm thick. The arrows indicate the two pressure end points of the plateau of the hysteresis loop. The inset shows a schematic representation of three possible configurations for pores of similar size, all having the same probability. The shading lines, the white regions, and the black triangles represent the condensed fluid, the vapor and hypothetical constrictions in the pores, respectively.

for sample A as a reference, all normalized to the same sample external surface as sample A, that is, to the same number of pores. The inset in Figure 7 shows the four isotherms normalized to the same pore volume.

For the samples 12.9 and 4.3 μm thick, thinned with a NaOH solution, we observe, at the end of the condensation process, the emptying of larger pores. This is due to the chemical dissolution of silicon walls separating neighboring pores, which gives rise to larger pores at the top of the layer.

If we disregard this superficial layer, the hysteresis loops corresponding to the abraded samples and to the as-prepared sample A are identical (inset of Figure 7). This shows that, if the hysteresis loops observed in p^+-type porous silicon are due to pore blocking effect, the hypothetical constrictions responsible for pore blocking are not located at the surface but randomly distributed along the pore axis.

The inset of Figure 8 represents schematically different possible configurations for pores of similar size, these configurations having the same probability. Along the "plateau" preceding the steep evaporation branch we should observe a decrease of the adsorbed amount corresponding to the emptying of the top of the pores with configurations (b) and (c) having diameter higher than the diameter of the largest constriction.

We have measured the decrease of the adsorbed amount along the plateau, using krypton at 77.4 K, which is more precise than with N_2 gas because krypton behaves as a perfect gas on the whole pressure range ($0 \leq P \leq P_0 = 1.76$ mmHg) of the isotherm measurements. It is not the case for N_2 at 77.4 K for which the perfect gas law correction must be known for each pressure along the plateau to make very precise measurements. Currently, the same perfect gas law correction factor is used for nitrogen at all pressures to determine the adsorbed amount, which introduces errors mainly at the highest pressures, precisely on the plateau.

Figure 8 represents the krypton isotherm at 77.4 K measured in a porous layer formed under the same conditions as sample A but 1 μm thick in order to enhance the contribution of the top of the pores with regard to the pore volume. The amount of gas desorbed between the two arrows in Figure 8 ($P/P_0 \simeq 0.6-0.85$) corresponds to 0.005 cm^3 STP, that is, 1.35×10^{17} atoms. These desorbed amounts come from the cell surface, the external surface of samples including the top of Si walls separating the pores, the formation of menisci at the top of pores, and possibly the emptying of the top of pores with configurations (b) and (c).

The surface area of our analysis cell is equal to $\sim$190 cm^2 and the geometical surface area of the sample prepared with a 2-in. Si wafer is ($2 \times 20-7.5$) cm^2 where 7.5 cm^2 is the surface area of pore sections. Typically, the amount of Kr atoms reversibly adsorbed on nonporous solids[2] between $P/P_0 = 0.6$ and $\sim$0.85 is equal to one monolayer (0.5×10^{15} atoms/cm^2). This corresponds to the desorption of 1.1×10^{17} atoms from the nonporous surface. The volume of menisci formed at the top of pores can be estimated from the pore density (see Table 1) and the mean pore diameter: it corresponds to $\sim 0.4 \times 10^{17}$ Kr atoms by assuming hemispherical menisci. Thus, the totality of the amount of gas desorbed along the "plateau" (1.35×10^{17} Kr atoms) originates in the desorption from nonporous surfaces and in evaporation from the top of pores (1.5×10^{17} Kr atoms).

This suggests that the plateau preceding the steep evaporation branch is not due to pore blocking effect caused by individual constrictions schematically represented in the inset of Figure 8.

Pore blocking effect was also questionned by Wallacher and co-workers.[22] According to these authors the hysteresis loop of type H2 observed in porous silicon is not due to "local pore blocking caused by individual constrictions of pore" but is rather the consequence of a strong disorder imposed by "large number of minor variations" in pore diameter. More recently, it has been proposed that any variation in the fluid/wall interaction along the pore (variations in pore size or shape, density of the porous material, chemical nature of the surface, etc.) can produce the same effect.[23] We have already noted in the Experimental Section that the Si walls contain many facets at a scale of a few atoms[14] which can be considered as a "strong disorder" as defined above.

At this stage of the paper, it is too early to take position in favor or against the explanations proposed in refs 22 and 23 since we must explain not only the shape of the boundary hysteresis loop but also the hysteretic behavior inside the main loop: the status of the hyteresis loop is connected to the problem of the independence of the pores. This problem is considered in the next section. The cause of the hysteresis loop will be discussed after.

3.2. Interaction Mechanism without Percolation Process. The asymmetry of the hysteresis loops (type H2) observed in p^+-type porous silicon is a first indication of the existence of an interaction mechanism between the pores during the evaporation process but not a proof.

(22) Wallacher, D.; Künzner, N.; Koralev, D.; Knorr, N.; Knorr, K. *Phys. Rev. Lett.* **2004**, *92*, 19.
(23) Puibasset, J. *J. Chem. Phys.* **2007**, *127*, 154701.

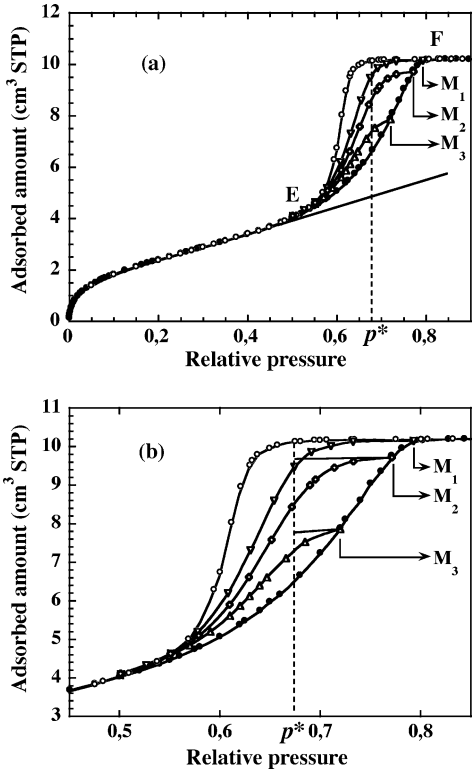

Figure 9. (a) Nitrogen adsorption isotherm at 77.4 K for sample A shown in Figure 6 with three PDSCs initiated at the reversal points M_1, M_2, and M_3. E and F are the end points of the boundary hysteresis loop. In the relative pressure range (0.1−0.5), the adsorbed amount increases pratically linearly with P/P_0 (see eq A4). The corresponding straight line has been continued at relative pressure higher than 0.5 to guide the eye. (b) Zoom of (a) in the hysteresis loop region. The lines without symbol are the PDSCs calculated using eq A10 corresponding to the points M_2 and M_3. The PDSC starting at M_1 coincides with the "plateau" of the boundary desorption branch. p^* represents the relative pressure above which no evaporation occurs from the porous system full of the condensed phase as expected in the independent pore model.[3]

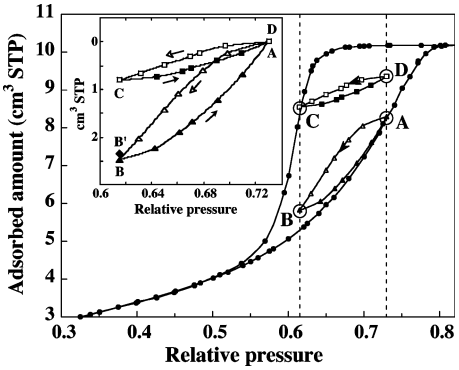

Figure 10. Hysteresis loop for sample A shown in Figure 6 with two subloops measured between the same pressure end points p_A and p_B, one (ABA) initiated on the primary filling branch, the other (CDC) on the primary draining branch. The inset shows the two subloops for which the right end points A and D are offset to overlap. The point B′ accounts for the correction as calculated in Appendix B. This correction represents less than 8% of the observed lack of congruence which is $V_{B'} - V_C = 1.66$ cm^3 STP.

To elucidate whether a porous system is composed of independent pores or not, it is necessary to study the behavior of the system inside the main loop. We have performed two different experiments presented below.

First, it is necessary to find which entity in a p^+-type porous silicon layer constitutes a domain as defined by Everett in ref 3, either "empty" with a film adsorbed on the pore walls or filled with the dense phase.

As we have seen in the Experimental Section, the cross-section area of each pores is almost constant. Anyhow, the variation of the cross-section area along the pore axis is much lower than the standard deviation of the PSD (13 ± 6 nm for sample A). Therefore, at a point of the condensation branch, a given pore fills in a relative pressure range δp much lower than Δp where $\Delta p = (0.8-0.5)$, $p = 0.5$, and $p = 0.8$ being the pressure end points of the boundary hysteresis loop of sample A (see Figure 6): $\delta p \ll \Delta p$. Thus, along the condensation branch we can consider that each tubular pore is either filled or "empty" and constitutes a domain.

3.2.1. Primary Descending Scanning Curves. We have measured a serie of PDSCs, that is, evaporation curves initiated at reversal points on the primary condensation curve.

Figure 9a shows the boundary hysteresis loop corresponding to sample A and three PDSCs initiated at the reversal points M_1, M_2, and M_3. According to the independent pore model,[3] a filled pore will not empty at a relative pressure higher than p^* whatever the position of the reversal point is, p^* being the pressure above which no evaporation occurs when the porous system is full of the dense phase. Therefore, for independent pores, only desorption from the pores not yet filled with the dense phase at M_1, M_2, and M_3, called the "empty" pores in the rest of the text, should be observed along the PDSCs at pressure higher than p^*. Thus, a quasi-linear variation of the adsorbed amount is expected as that observed before capillary condensation occurs but with a lower slope since the number of "empty" pores is lower.

In Appendix A, we have calculated the PDSCs expected from a system of independent pores by estimating $\Delta v_M(p)$, the amount of gas desorbed from the pores still "empty" at a reversal point M.

Figure 9b is a zoom of Figure 9a in the hysteresis loop region. The lines without symbol are the PDSCs, corresponding to the reversal points M_2 and M_3, calculated using eq A10. The PDSC starting at M_1 coincides with the "plateau" of the boundary desorption branch.

For the three PDSCs, these estimates show that the major part of the amount desorbed at the pressure p^* comes from evaporation. Qualitatively, one observes that the evaporation pressure of a pore depends on the extent to which the porous system is filled. The pores in p^+-type porous silicon do not drain independently of one another.

3.2.2. Subloops. To confirm these results, we have compared two subloops within the boundary loop between the same limiting pressures, the one (ABA) initiated on the primary filling branch, the other (CDC) on the primary draining branch (see Figure 10). The inset of Figure 10 shows the two subloops for which the right points A and D are offset to overlap. For a system composed of independent pores these two subloops should be superimposable, i.e., congruent,[3] which is clearly not the case for porous Si layers. Note that a correction must be brought to the subloops to account for the presence of an adsorbed film on the surface of the "empty" pores.[19] Indeed, this test can be rigorously applied only for systems composed of two-state microsystems which is not the case for adsorption in porous materials: a pore is not filled or empty but filled or "empty" with a film on the pore walls, the thickness of which depends on the pressure. Figures 6 and 7 in our previous paper[19] show that a certain number, n, of pores remains filled along (CDC) and "empty" along (ABA). To determine the actual lack of congruence we must estimate

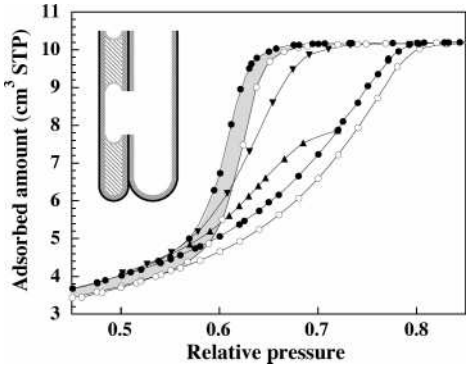

Figure 11. Magnification of the hysteresis loop region of N_2 adsorption isotherm performed at 77.4 K for sample A with pores closed at one end (●) and for the corresponding membrane with pores open at both ends (○), together with two PDSCs shown in Figure 10. The zone between the two evaporation branches has been colored in gray. The inset shows a schematic representation of two interconnected neighbor pores, one filled with the dense phase (hatched part), the other "empty" covered by an adsorbed film, at a reversal point on the condensation branch. This intersecting region divides the filled pore into two parts. The upper and lower parts of the filled pore should empty as a pore open at both ends and a pore closed at one end, respectively, and the PDSCs should be located within the gray zone.

Δv_n(AB), the amount of gas desorbed from these n "empty" pores along the path AB. As shown in Appendix B, we find $\Delta v_n(\mathrm{AB}) \lesssim 0.13$ cm^3 STP. In the inset of Figure 10, this amount has been added to V_B, the adsorbed amount at B, to obtain the corrected point B′. This correction represents less than 8% of the observed lack of congruence $V_{B'} - V_C = 1.66$ cm^3 STP.

3.2.3. Relevance of Percolation Process. The interaction mechanism generally invoked to explain such results is percolation. In previous experiments,[1] we have looked for the presence of interconnections between the pores. The experiment consisted in thermally oxidizing a sample A, a part of which being masked by an aluminum cap to prevent oxygen from entering the porous layer from the top of the pores. We have found that oxygen did not invade the pores located under the aluminum cap. This result shows that if there are interconnections they are not numerous enough to lead to percolation process in this porous medium.

Nevertheless, as the pore blocking/percolation model is the only interaction mechanism proposed up to now to explain the adsorption−desorption process in connected pores, it is important to discuss the influence of hypothetical interconnections on the evaporation process in such a porous medium.

In inset of Figure 11 we have represented two interconnected neighbor pores, one filled, the other "empty", at a reversal point on the condensation branch. If the interconnection has a size smaller than that of the filled pore, it will empty at a lower pressure and hence will not disturb the emptying of the filled pore. For an interconnection having a size higher than that of the filled pore, which is the case represented in inset of Figure 11, the intersecting region will empty at a pressure higher than that of the filled pore, dividing the filled pore into two regions: an upper part, open at both ends which will empty as a pore open at both ends, and a lower part, closed at one end which will empty as a pore closed at one end. In Figure 11, we show the two nitrogen hysteresis loops for sample A and its corresponding membrane. As previously observed,[1] they are distinct but both of them are of type H2. In these conditions, even if the pores are connected, we should have observed PDSCs resembling the boundary evaporation branches and located between them within the gray zone shown in Figure 11. This is far from the case.

The above results show that the pores of p^+-type porous silicon strongly interact with one another during the evaporation process, but the interaction mechanism is not percolation.

4. Discussion

We have shown in the previous sections that the hysteresis loop of type H2 observed in p^+-type porous silicon is not due to the presence of constrictions in the pores. Moreover, the pores of this porous material strongly interact with one another during the evaporation process and the interaction mechanism is not percolation. The pores of porous silicon are coupled even though they are not connected.

Calculations via mean field density functional theory and Monte Carlo simulations for a lattice-gas model[24−26] reproduce qualitatively the hysteresis physical features associated with capillary condensation in disordered porous material such as silica gel or porous glass, features which are similar to that found in p^+-type porous silicon. Guided by these calculations, it has been proposed, in recent papers, that the H2 hysteresis loop observed in p^+-type porous silicon is the consequence of a strong disorder in each pore imposed by some variations along the pore axis of the pore diameter[22] or in the fluid/wall interaction.[23] The idea is the following. Due to the presence of topological or chemical heterogeneities along the pore axis, a pore is composed of numerous domains so that it does not fill (or empty) at a given pressure. During the filling (or the emptying) of a pore, the numerous domains interact producing a dissymmetry between the adsorption and desorption branches (type H2).[23] In this approach, the pores of porous silicon are independent from one another, the disorder in each pore divides the pore into domains and is supposed to be responsible for the H2-type hysteresis loop. Note that these calculations[23] have been performed in a cylindrical pore of 3 nm diameter, the length of the interaction fluid/substrate being cut at 0.75 nm. In pores with diameters of 13 nm for sample A and of 26 nm for sample B, the effect of chemical heterogeneities is expected to be drastically reduced compared to that in a pore of 3 nm diameter.

This approach cannot explain our whole results. If disorder must be invoked, it must be looked for in the large PSD rather than within each pore. The problem is the following. In what relative pressure range (δp) along the wide condensation branch does a given pore fill? As we have already noted, the pore sections are undoubtly not constant along the pore axis but their variation is certainly very small with regard to the standard deviation of the PSD (remember that a 2D binary image well reproduces both the consistancy in the Si wall thickness and the porosity). The presence of topological or/and chemical heterogeneities can favor the formation of liquid bridges, and at this moment the pore is not fully filled but it is likely that this situation extents within a pressure range δp small compared to the pressure range Δp corresponding to the filling of the whole porous material: $\delta p \ll \Delta p$. We can hence reasonably suppose that a pore in porous silicon constitutes a domain. At a reversal point of the condensation branch, M_3 in Figure 9 for instance, the major part of pores is either filled or empty. In the approach of J. Puibasset, the hysteresis loop corresponding to an assembly of pores is the sum of the individual hysteresis loops. Thus, when the evaporation is commenced while the porous system is partially filled, the hysteresis loop obtained should be of type H2, which is not the case. The results represented in Figures 9 and 10 show that the

(24) Kierlik, E.; Monson, P. A.; Rosinberg, M. L.; Sarkisov, L.; Tarjus, G. *Phys. Rev. Lett.* **2001**, *87*, 055701.
(25) Rosinberg, M. L.; Kierlik, E.; Tarjus, G. *EuroPhys. Lett.* **2003**, *62*, 377.
(26) Sarkisov, L.; Monson, P. A. *Phys. Rev. E* **2002**, *65*, 011202.

evaporation of a pore depends strongly on the state of the neighbor pores that is whether they are filled or empty. This is the problem Mason attempted to solve by proposing his pore blocking/percolation model.[5,6] In porous silicon there is no pore blocking and no percolation while there is a coupling between the pores, a phenomenon which cannot be explained by the disorder in each pore.

If we disregard the boundary hysteresis loops, the shape of which depends on the porous material, H1 for MCM-41 and SBA-15, H2 for porous glass and p^+-type porous silicon, the hysteretic features inside the main loop are qualitatively the same for all these porous systems. Recent studies on MCM-41 and SBA-15[19,27,28] revealed that the PDSCs in these materials resemble that observed in disordered porous material[7] and in p^+-type porous silicon. For SBA-15 we have shown that two subloops between the same pressure end points are not congruent, which proves unambiguously that the pores of SBA-15 do not evaporate independently of one another.[19]

Comparing the hysteretic behavior of SBA-15 and of KIT-16, an ordered mesoporous silica which consists of a three-dimensional (3D) network of interconnected pores of almost cylindrical shape and same size, Morishige and co-workers[29] noted that despite a large difference in porous structure, the shape, and thermal behavior of the adsorption hysteresis for KIT-16, as well as the sorption scanning behavior, were indistinguishable from those of SBA-15. This indicates that interconnections among pores of KIT-16 do not have a significant effect on the adsorption hysteresis.

In summary, in all these porous materials we have considered, the pores interact whether they are connected or not and whatever the shape of hysteresis is, H1 or H2. From now on the question is what physical parameter couples the pores?

5. Conclusion

We have presented and discussed measurements of boundary hysteresis loops, reversal curves and subloops in p^+-type mesoporous silicon. This porous material is composed of tubular pores perpendicular to the Si substrate. The average direction of the pores is identical to within $\pm 0.1°$ of the [100] crystal axis. The polygonal cross-section areas of pores are almost constant. In this porous material we have found wide hysteresis loop of type H2. We have shown that the irreversibility of the condensation−evaporation process is not due to the presence of constrictions. The pores are not connected so that this material should behave as an assembly of independent pores. It is not the case. The asymmetry of the hysteresis loops together with the shape of the primary descending scanning curves and the large lack of congruence between subloops with the same pressure end points prove the existence of strong interactions between the pores during the evaporation.

It is noteworthy that the hysteretic behavior observed in porous silicon is quite similar to that shown in porous glass which is classified as disordered porous material. Moreover, we have shown recently that the cylindrical pores of SBA-15 material, which exhibits a boundary hysteresis loop with two-steep parallel branches (type H1), do not either evaporate independently of one another. It appears that the interdependence between the pores is a feature common to all the porous materials whether interconnections are present or not and whatever the type of hysteresis is H1 or H2. The physical parameter which couples the pores must be common to all these porous materials.

In a previous paper,[1] we proposed that the continuous liquid film which covers the top of the pores in the p^+-type porous silicon layers at the end of the pore filling, and hence connects the pores, could play a role in the desorption process by preventing the concave menisci from passing through each pore at the expected equilibrium pressure. Results presented elsewhere[18] invalidate this idea.

Therefore, the last coupling parameter which we must consider is the porous matrix itself. In a subsequent paper[17] we shall analyze the effect of the elastic deformation of the porous matrix on the adsorption−desorption cycle, a parameter which has been ignored in practically all the theoretical treatments of physisorption.

Finally, the experimental results presented here show that the IUPAC classification which associates the shape of the boundary hysteresis loop to a given morphology, H1 for an assembly of non connected cylindrical pores and H2 for disordered and highly connected system, must be reconsidered. The difference between the hysteresis loops of type H1 and H2 could be simply that H1 is characteristic of a narrow PSD, H2 of a large PSD, whatever the shape of the pores is and whether they are connected or not.

Appendix A. Calculated PDSC for a System of Independent Pores (Figure 9)

Small letters define the amount of adsorbate in the "empty" pores, and capital letters the total adsorbed amount including the adsorbate in the "empty" pores and the condensate in the filled pores. The pore volumes are noted ϑ^{pores}.

To a first order in the calculation, the adsorbed amount before capillary condensation (all the pores are "empty") may be written

$$v(p) = \alpha L \sum_i n_i l_i t(p) \tag{A1}$$

where n_i is the number of pores with perimeter l_i, $t(p)$ the film thickness versus the relative pressure p, L the pore length, and α a constant. Introducing $\langle l \rangle$ and $\langle s \rangle$, the mean values of the perimeter and of the pore surface area, eq A1 becomes

$$v(p) = \alpha NL\langle l \rangle t(p) = \alpha \vartheta_{\text{tot}}^{\text{pores}} \frac{\langle l \rangle}{\langle s \rangle} t(p) \tag{A2}$$

where $\vartheta_{\text{tot}}^{\text{pores}} = NL\ \langle s \rangle$ is the pore volume.

We have seen in the Experimental Section that the mean pore diameters defined by $\langle D \rangle = \langle l \rangle / \pi$ and $\langle D \rangle = \sqrt{4\langle s \rangle / \pi}$ are equal. Equation A2 then becomes

$$v(p) = \alpha' \frac{\vartheta_{\text{tot}}^{\text{pores}}}{\langle D \rangle} t(p) \tag{A3}$$

Thus, to a first order in the calculation, $v(p)$, the amount of gas adsorbed before the capillary condensation occurs, is (i) equivalent to that adsorbed in pores of an unique size equals to the mean size of the distribution (∼13 nm for sample A and ∼26 nm for sample B), (ii) proportional to the pore volume, and (iii) inversely proportional to the mean pore diameter. The latter property (iii) is illustrated in Figure 6 where it is shown that $v(p)$ is lower for sample B than for sample A once the isotherms are normilized to the same pore volume.

We have experimentally found that the adsorbed amount $v(p)$ in the pressure range (0.1−0.5) increases pratically linearly with p (regression coefficient: 0.999), with an adsorption rate equals

(27) McNall, M.; Laurence, R. L.; Conner, C. W. *Microporous Mesoporous Mater.* **2001**, *44*−*45*, 709.
(28) Esparza, J. M.; Ojeda, M. L.; Campero, A.; Dominguez, A.; Rojas, F.; Vidales, A.; Lopez, R. H.; Zgrablich, G. *Colloids Surf. A: Physicochem. Eng. Aspects* **2004**, *241*, 35.
(29) Morishige, K.; Noriko Tarui, N. *J. Phys. Chem. C* **2007**, *111*, 280.

to 5.25 cm^3 STP.p^{-1} for a pore volume $\vartheta_{tot}^{pores} = 10.15$ cm^3 STP, so that

$$v(p) = v(0.1) + 5.25p \tag{A4}$$

This straight line, represented in Figure 9a, has been continued at pressure higher than 0.5 to guide the eye.

From eqs A3 and A4, we get

$$dt(p) = \frac{5.25\,\langle D\rangle}{\alpha'\vartheta_{tot}^{pores}}\,dp \tag{A5}$$

Applying eq A3 to the pores still "empty" at point M of the condensation branch, we find

$$v_M(p) = \alpha'\frac{\vartheta_M^{pores}}{\langle D_M\rangle}\,t(p) \tag{A6}$$

where ϑ_M^{pores} is the volume of pores still "empty" at the reversal point M and $\langle D_M\rangle$, their mean diameter.

From eqs A3, A4, and A6, we can estimate $\Delta v_M(p)$, the amount of gas desorbed from the pores still "empty" at M

$$\Delta v_M(p) = v_M(p_M) - v_M(p) = 5.25\left(\frac{\vartheta_M^{pores}}{\vartheta_{tot}^{pores}}\right)\left(\frac{\langle D\rangle}{\langle D_M\rangle}\right)(p_M - p) \tag{A7}$$

As the mean pore diameter of the "empty" pores, $\langle D_M\rangle$, is higher than the mean pore diameter of all the pores, $\langle D\rangle$, eq A7 overestimates the amount of gas desorbed from the "empty" pores

$$\Delta v_M(p) < 5.25\left(\frac{\vartheta_M^{pores}}{\vartheta_{tot}^{pores}}\right)(p_M - p) \tag{A8}$$

The ratio $\vartheta_M^{pores}/\vartheta_{tot}^{pores}$ varies from 1 to 0 when the porous system fills with the dense phase (from point E to point F in Figure 9a).

To estimate $\vartheta_M^{pores}/\vartheta_{tot}^{pores}$, we have used a linear approximation with regard to $(\vartheta_{tot}^{pores} - V_M)$

$$\vartheta_M^{pores}/\vartheta_{tot}^{pores} \approx f = \frac{(\vartheta_{tot}^{pores} - V_M)}{(\vartheta_{tot}^{pores} - V_E)} \tag{A9}$$

where V_M and V_E are the adsorbed amounts at a reversal point M and at point E where the pores begin to fill. Finally, we obtain

$$\Delta v_M(p) \approx 5.25 f(p_M - p) \tag{A10}$$

Figure 9b shows the PDSCs calculated using eq A10 corresponding to the reversal points M_2 ($f = 0.07$) and M_3 ($f = 0.38$). The PDSC starting at M_1 coincides with the "plateau" of the boundary desorption branch.

Appendix B. Correction for Two Subloops between the Same Pressure End Points (Figure 10)

As we have previously shown[19] and recalled in Section 3.2 of this paper, for a system of independent pores a certain number, *n*, of pores remain filled along the subloop (CDC) and "empty" with a film on the pore walls along the subloop (ABA). In this appendix we estimate Δv_n(AB), the amount of gas desorbed from these *n* "empty" pores along the path AB.

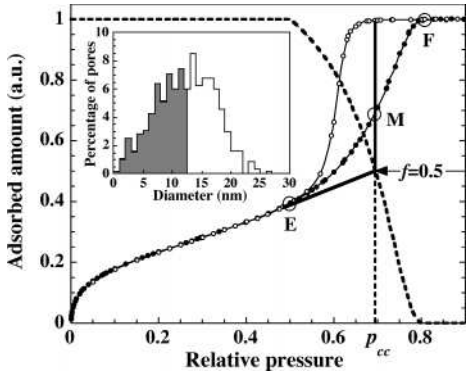

Figure 12. N_2 Adsorption isotherm for sample A shown in Figure 6 normilized to a unit adsorbed amount and the corresponding PSD (inset). The solid line represents the calculated isotherm adsorption for an "ideal" system composed of pores of an unique size equals to the mean size of the distribution (13 nm). At p_{cc}, the capillary condensation pressure of this system, 50% of the pore volume of sample A is still "empty" but covered with an adsorbed film. The fraction of these pores still "empty" are represented in white in the PSD. The dash line represents *f*, the fraction of pores still "empty" at p_{cc}, calculated according to eq A9, as a function of the relative pressure.

We apply eq A8 to these "empty" pores

$$\Delta v_n(\mathrm{AB}) < 5.25\left(\frac{\vartheta_n^{pores}}{\vartheta_{tot}^{pores}}\right)(p_A - p_B) \tag{B1}$$

where ϑ_{tot}^{pores} and ϑ_n^{pores} are the pore volume and the volume of the *n* "empty" pores, respectively.

The difference between ϑ_n^{pores} and $v_n(p_A)$, the amount adsorbed in the *n* "empty" pores at pressure p_A, can be expressed as a function of $V_D - V_A$

$$V_D - V_A = \vartheta_n^{pores} - v_n(p_A) = 1.07\ \mathrm{cm^3\ STP} \tag{B2}$$

where V_D and V_A are the adsorbed amounts at points D and A (see Figure 10), respectively.

An estimation of the upper limit of the fraction $v_n(p_A)/\vartheta_n^{pores}$ provides a second equation to obtain ϑ_n^{pores}.

We have replaced the real porous system by an "ideal" system composed of identical pores having a diameter of 13 nm, the mean value of the PSD, and estimated the ratio $v(p_{cc})/\vartheta_{tot}^{pores}$ corresponding to this "ideal" system where $v(p_{cc})$ is the adsorbed amount just before the fluid in a pore of diameter of 13 nm capillary condenses and ϑ_{tot}^{pores}, the pore volume. As the mean size of the *n* pores "empty" along (ABA) and filled along (CDC) is larger than the mean size of the distribution and as, by definition, they did not yet capillary condense, $v(p_{cc})/\vartheta_{tot}^{pores}$ constitutes an upper limit of $v_n(p_A)/\vartheta_n^{pores}$.

p_{cc} can be estimated as follows. Let us call *M* the point of the condensation branch at which a pore of diameter of 13 nm fills (see Figure 12). At $p = p_{cc}$, we have $\vartheta_M^{pores}/\vartheta_{tot}^{pores} = 50\% \approx f$, where ϑ_M^{pores} is the volume of the pores still "empty" at *M* and *f* is defined by eq A9. Thus, p_{cc} is determined by the equation $f = 0.5$. In Figure 12 are represented the isotherm for sample A normalized to a unit adsorbed amount, the corresponding PSD with the pores still "empty" at $p = p_{cc}$ together with the function *f*. The graphic solution of the equation $f = 0.5$ gives $p_{cc} = 0.7$.

It remains to estimate $v(p_{cc})$. Remember that, for $p \leqslant 0.5$, the amount adsorbed in the ideal system is, to a first order in the

calculation, equal to $\sim v(p)$ the amount adsorbed in the real system (see eq A3). The continuation until $p_{cc} = 0.7$ of the linear fit representing the adsorbed amount between 0.1 and 0.5 allows the estimation of $v(p_{cc})$. We find $v(p_{cc} = 0.7) = 5$ cm^3 STP.

Thus, for 13 nm pores, the ratio of the adsorbed amount just before the capillary condensation occurs over the pore volume is estimated to about 0.5. Therefore, $v_n(p_A) < 0.5\ \vartheta_n^{pores}$ and eq B2 becomes $\vartheta_n^{pores} < 2(V_D - V_A)$, i.e., $\vartheta_n^{pores} < 2.14$ cm^3 STP. Thus, the volume of these *n* pores is lower than 21% of the total pore volume. According to eq B1, the amount of gas desorbed from these "empty" pores between the pressures p_A and p_B, Δv_n-(AB), is then lower than $0.21 \times 5.25 \times (p_A - p_B) \simeq 0.13$ cm^3 STP. This amount must be added to V_B, the adsorbed amount at point B, to obtain the corrected point B′ as shown in inset of Figure 10.

LA703978V